J. Phys. B: At. Mol. Opt. Phys. 24 (1991) 1003–1016. Printed in the UK

Single electron capture for impact of (0.5–9 keV) C^{2+} on He, Ar and H_2

E Unterreiter, J Schweinzer and H Winter

Institut für Allgemeine Physik, Technische Universität Wien, Wiedner Hauptstrasse 8-10, A-1040 Wien, Austria

Received 31 October 1990

Abstract. Absolute total cross section measurements and state-selective translational energy spectroscopy have been performed for single electron capture by 0.5–9 keV C^{2+} from H_2, He and Ar, for the C^{2+} ground state as well as the C^{2+} metastable state. The experimental results are compared with available data obtained with undefined metastable primary ion beam fractions. For the particular case of C^{2+}–H_2 collisions, experimental results could be explained by close-coupling calculations involving empirically derived coupling matrix elements and Franck–Condon factors for H_2 ionization via electron capture.

1. Introduction

The important role of electron capture by multiply charged impurity ions in the boundary region of tokamak discharge plasmas is nowadays fully acknowledged (Stangeby and McCracken 1990). In present day magnetically confined plasma fusion experiments, usually carbon is by far the dominant impurity species. An assessment of the importance of electron capture reactions for both energy balance and transport in the boundary plasma is greatly inhibited by a severe lack of reliable absolute electron capture cross sections (Tawara and Phaneuf 1988, Gilbody *et al* 1989, Janev *et al* 1989, Tawara and Fritsch 1989). Furthermore, the existence of metastable primary ion states is a notorious source of great uncertainty for such measurements, since in the vast majority of cases the corresponding metastable ion beam fractions have not quantitatively been taken care of (Aumayr and Winter 1989).

In the present study we investigate single electron capture by C^{2+} ions, which can be present in their $(2s^2)\ ^1S$ ground state as well as in the metastable $(2s2p)\ ^3P^o$ state. As targets we consider the fusion-relevant species H_2 and He (Janev *et al* 1988). Furthermore, we have also investigated C^{2+}–Ar collisions, for which single electron capture involves reaction channels with nearly equal energy defects as for C^{2+}–H_2 collisions, because of the nearly equal target ionization potentials (15.76 eV for Ar (cf Bashkin and Stoner 1975) compared with 15.42 eV for H_2 (Herzberg 1950)). However, in contrast to Ar for the H_2 molecule Franck–Condon factors might also influence the probability of electron capture, apart from the reaction energy defects for particular capture channels.

The present work involves both determination of the total electron capture cross sections and state-selective measurements by means of translational energy spectroscopy.

0953-4075/91/051003+14$03.50

2. Experimental methods

2.1. Primary C^{2+} ion beam production and determination of the metastable $C^{2+}(1s^2 2s2p)\ ^3P^o$ fraction

C^{2+} ions have been obtained from a Nier-type ion source, involving electron impact on CH_4. As compared with CO or CO_2, CH_4 was found to be more appropriate because of the smaller energy spread of the resulting C^{2+} ions, which determines the achievable energy resolution of translational energy spectra (see section 2.3).

The extracted ions were accelerated, magnetically mass selected and guided to the collision chamber (cf figures 1(*a*) and (*b*)).

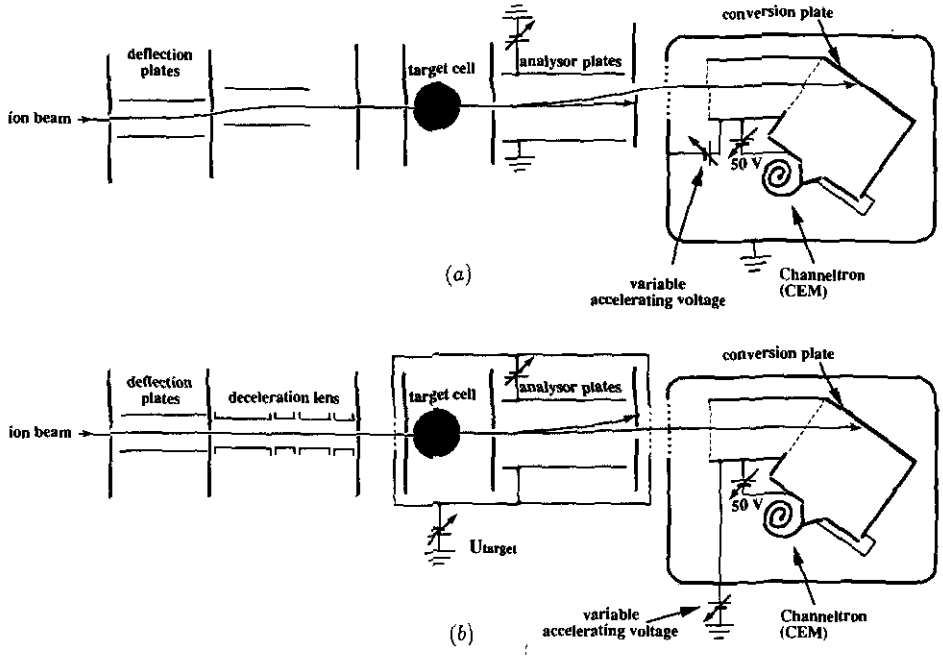

Figure 1. Schematic layout of experimental set-ups for (*a*) ion beam attenuation measurements and (*b*) total SEC cross section measurements.

Besides the ground state $C^{2+}(2s^2)\ ^1S$, there exists one long-lived ($\tau = 12.5$ ms, Cheng *et al* 1979) excited (metastable) $C^{2+}(2s2p)\ ^3P^o$ state (excitation energy 6.49 eV above the ground state (Bashkin and Stoner 1975)). The C^{2+} metastable ion beam fraction could be controlled by the ion source electron impact energy E_e. It disappeared for $E_e \leqslant 70$ eV, as shown by translational energy spectra at various electron impact energies (see below), and approached an apparently constant value for $E_e \geqslant 150$ eV. The metastable ion fraction could be determined by means of an attenuation method as used by Turner *et al* (1968) in the following way.

The attenuation of an ion beam current I_0 consisting of two components only, i.e. the ground state and one metastable state, which feature different attenuation cross sections σ_g and σ_m in a particular attenuation gas, follows the relation

$$I(\pi) = f_g I_0 \exp(-\sigma_g \pi) + f_m I_0 \exp(-\sigma_m \pi) \tag{1}$$

with π the target thickness of the attenuation gas, I_0 the ion current at zero target thickness and f_g and f_m the fractions of ground state and metastable ions, respectively. The attenuation of both ion beam components needs to be mutually independent (Gilbody 1978). A semilog plot of I/I_0 against target thickness shows a linear slope $\sigma_g \pi$ for the pure ground-state ion beam, whereas for a mixed beam two decay slopes can clearly be distinguished if the two attenuation cross sections are sufficiently different.

Our experimental set-up used for these attenuation measurements is shown in figure 1(*a*). Before entering the collision chamber the ion beam was cleaned from charge-exchanged species by a set of deflection plates. The pressure in the collision chamber was measured by a Baratron pressure gauge connected behind a needle valve to the gas inlet system. Only relative pressure measurements have been necessary, since from the attenuation curve the two ion beam fractions could be obtained via extrapolation to zero pressure. By means of condenser plates immediately behind the collision chamber the ions were directed through an offset aperture, to avoid disturbance of the attenuation measurements from charge-exchanged species.

The experimental set-up has been tested by measuring the well established metastable fractions of Ar^{2+} ^1D, ^1S in Ar^{2+} ion beams produced from the Nier-type ion source at 80 eV electron impact energy. Attenuation of Ar^{2+} in He showed a 65% fraction of ^3P ground-state ions, in good agreement with results from Nakamura *et al* (1985).

Typical attenuation curves for C^{2+} in He as attenuation gas are shown in figure 2. Note, that for C^{2+} the corresponding σ_g and σ_m values differ by about one order of magnitude (cf table 1). The open circles in figure 2 show the attenuation curve for a pure ground-state C^{2+} beam produced with $E_e = 70$ eV, whereas the full symbols belong to a mixed beam ($E_e = 250$ eV). In the latter case, I/I_0 drops rapidly at low target gas pressure, but toward higher pressure gradually converges to the same slope as for the pure ground-state ion beam (open symbols). Extrapolation of this slope toward zero target gas pressure yields the ground-state ion beam fraction at the intersection with the ordinate (figure 2), from which a metastable fraction of $f_m = 10\% \pm 1\%$ could be deduced.

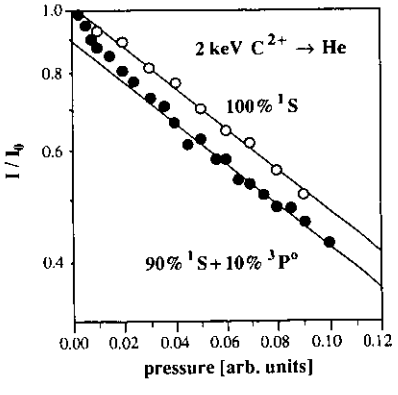

Figure 2. Typical attenuation curve for C^{2+} ion beams in He. Open symbols refer to attenuation for a pure ground state ion beam produced at $E_e = 70$ eV, and full symbols show the attenuation characteristics for a mixed beam ($E_e \geq 150$ eV), from which a metastable fraction of 10% can be deduced.

Table 1. Total single electron capture cross sections in 10^{-16} cm^2 for respectively $(2s^2)\ ^1S$ ground-state and $(2s2p)\ ^3P^o$ metastable C^{2+} ions colliding with H_2 and He, vs impact energy. For both targets as well as Ar SEC cross sections for a 'mixed' ion beam with 10% metastable fraction have been given.

C^{2+}	H_2			Ar	He		
$(2s^2)\ ^1S$	100%	90%	—	90%	100%	90%	—
$(2s2p)\ ^3P^o$	—	10%	100%	10%	—	10%	100%
E (keV)							
0.6	4.27	7.88	40.32				
0.8	4.9	8.41	40.00			2.02	
1.0	5.6	8.72	36.75			2.20	
1.2	5.67	9.03	39.27				
1.4	6.02	9.34	39.27			2.15	
1.6	6.44	9.24	34.44			2.38	
1.8	6.85	9.98	40.53				
2.0	7.00	10.50	42.00	11.0	1.07	2.59	13.75
2.5	7.49	11.03	42.84				
2.75					1.16	2.72	14.16
3.0	8.26	11.33	38.95		1.19	2.77	14.37
4.0	9.24	11.85	35.38		1.41	2.88	13.62
5.0	9.73	12.56	38.01	12.6		3.11	
5.5					1.53	3.14	14.91

2.2. Measurement of total SEC cross sections

These measurements have been performed with a modified version of the technique described by Schweinzer and Winter (1990a). To improve the intensity of our primary C^{2+} ion beam at lower impact energy, addition of a deceleration lens permitted ion transport at relatively high energy with subsequent deceleration in front of the target chamber (cf figure 1(*b*)). The latter was adequately biased for the desired ion impact energy. The background pressure in the collision chamber of 1×10^{-7} mbar increased up to 2×10^{-6} mbar if target gas at a pressure of 1×10^{-4} mbar was introduced into the collision cell.

Immediately behind the collision cell, charge-exchanged singly charged ions were separated from the remaining doubly charged primary ions by means of a parallel-plate condenser field. The detection unit (Schweinzer and Winter 1990a) could be biased to ensure all ions hit the conversion plate with a fixed impact energy of 6 keV, irrespective of the chosen collision energy and ion charge state, thus avoiding collision energy-dependent detection efficiency. Total capture cross sections have been derived from the detector signal rates in the usual way (Aumayr and Winter 1985, Aumayr *et al* 1986, Schweinzer and Winter 1990a), with the target thickness determined by calibration to the well established absolute total electron capture cross sections for H^+-H_2 collisions at 4 keV impact energy (Stier and Barnett 1956).

2.3. Translational energy spectroscopy for state-selective electron capture measurements

A detailed description of our translational energy spectrometer has been given by Schweinzer and Winter (1989) and Aumayr *et al* (1989).

The primary C^{2+} ions were produced as described above. All translational energy spectra (TES) presented have been measured with an angular acceptance of 0.3° for the scattered, charge-exchanged ions. The achieved energy resolution of about 0.7 eV FWHM resulted in first place from the energy spread of the primary C^{2+} ion beam (cf above).

For C^{2+} electron impact production from molecular gases we assume Franck–Condon type transitions into highly excited molecular states during a direct ionization process. Consequently, the energy spread of the ions produced depends on the shape of the molecular potential surface and the position of relevant Franck-Condon transitions (Armenante *et al* 1985). If such transitions end up above the dissociation limit, all ions are produced with kinetic energies larger than zero, with the excess energy being released as kinetic energy of the fragments. The final kinetic energy of these fragments seems to be determined by momentum conservation only. For this reason CH_4 was found most suitable as the ion source feeding gas, causing production of C^{2+} beams with the smallest achievable kinetic energy spread.

Calibration of the scattered ion kinetic energy scale for TES was straightforward with Ar and He target gases, since the resulting C^+ peaks were well separated and corresponded to clearly distinguishable reaction channels. In the case of the H_2 target, the corresponding TES had to be calibrated at each collision energy by additionally introducing He into the target cell. Since the masses of both H_2 and He are comparably small with respect to C^{2+} ions, the kinetic energy scale of He-related TES could serve for calibration of TES for collisions with H_2. The error of this energy scale calibration can be estimated from approximate calculations of the scattering angle of the charge-exchanged ions and the resulting kinematic shifts for both targets (Jellen-Wutte *et al* 1985), leading to a maximum shift of the energy scale for $C^{2+}+H_2$ by 0.1 eV toward more exothermic values as compared with $C^{2+}+He$.

3. Presentation of results and discussion

3.1. Total SEC cross sections

As already mentioned in section 2.1, the metastable fraction in the C^{2+} primary ion beam could be controlled via the electron impact energy E_e. With $E_e = 70$ eV a pure $C^{2+}(2s^2)\ ^1S$ ground state beam was produced, whereas for $E_e \geq 150$ eV the 'mixed' beam contained a metastable fraction of 10%. Absolute electron capture cross sections have been measured with pure ground-state beams (σ_g) as well as with mixed beams (apparent cross section σ_{mix}). From both results the SEC cross section σ_m for the metastable primary ions could be simply deduced

$$\sigma_m = \frac{\sigma_{mix} - (1 - f_m)\sigma_g}{f_m}. \tag{2}$$

Total errors for σ_g (ground-state primary ions) are dominated by the applied calibration cross sections (±10%, cf section 2.2). Statistical errors of our measurements are about 5%. Since the mixed beam contained only a 10% metastable ion fraction, errors for σ_m derived according to equation (2) could increase up to 24% (50% confidence limits). Table 1 gives the such determined electron capture cross sections for C^{2+} (^1S, $^3P^o$)–He, Ar, H_2 collisions.

Figures 3 and 4 compare our results for C^{2+}–He and C^{2+}–H_2 collisions with data from other groups, which all apply to mixed ion beams with unspecified metastable

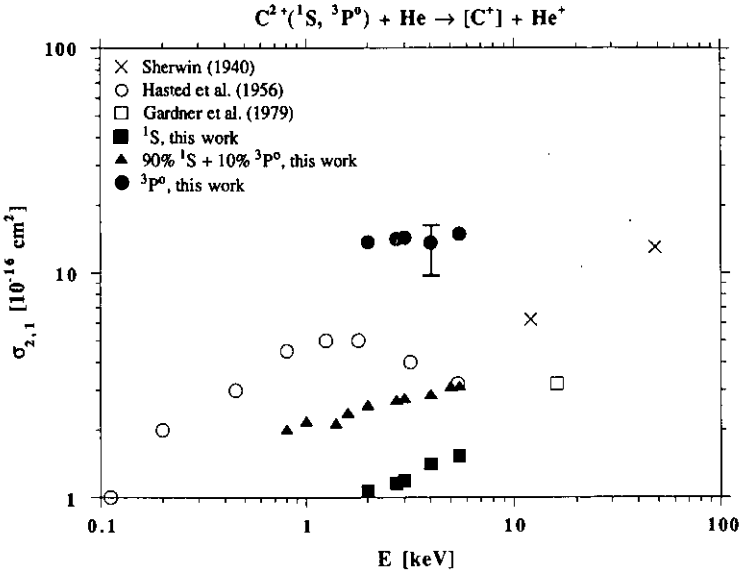

Figure 3. Total SEC cross sections $C^{2+}+He$ (full symbols) in comparison with results of other groups. Error bars give total errors for 50% confidence limit. For ground-state ions and the mixed beam the errors remain smaller than the respective symbol size.

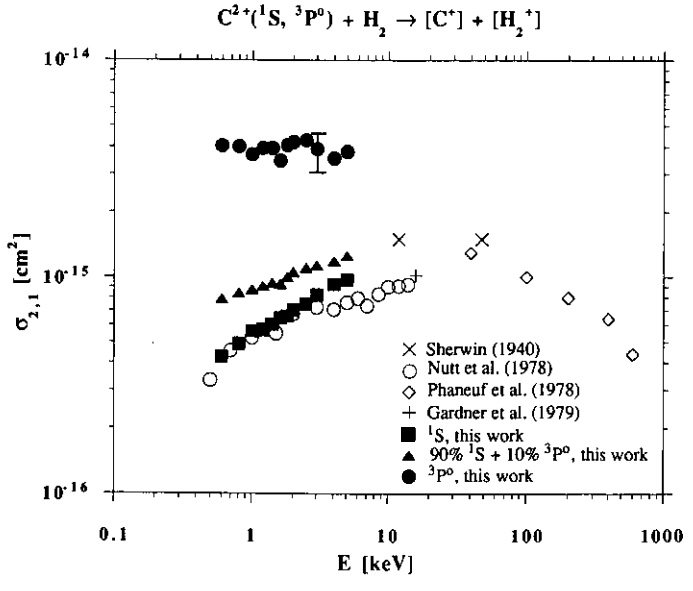

Figure 4. Total SEC cross sections $C^{2+}+H_2$ (full symbols) in comparison with results of other groups. Error bars as for figure 3.

fractions. Sherwin (1940) gave only two data points and stated a nearly linear variation of the cross sections with impact energy. As apparent from figure 3, the cross sections of Hasted and Smith (1956) are larger than our mixed beam cross sections, indicating that their primary ion beam metastable fraction was probably larger than ours. The single data point of Gardner *et al* (1979) fits well into our mixed beam cross sections for C^{2+}-He (figure 3), but agrees with our ground-state cross sections for C^{2+}-H_2 (figure 4). The data for C^{2+}-H_2 of Nutt *et al* (1978) are similar to our ground-state data, especially in the low impact energy range. At higher impact energy our data join smoothly into those of Phaneuf *et al* (1978).

3.2. State-selective measurements for C^{2+}-He

Figure 5 shows translational energy spectra (TES) for C^{2+}-He collisions taken at ion impact energies of 4 and 9 keV with a 10% metastable C^{2+} $^3P^o$ fraction. The peaks for reaction channels involving metastable primary ions have been shaded. For impact energies below 4 keV no further significant changes of the TES have been found. For the whole ion impact energy range the reaction channel

$$C^{2+}(2s2p)\ ^3P^o + He \rightarrow C^+(2s^22p)\ ^2P^o + He^+ + 6.3\ eV$$

is by far the dominant one, despite the small metastable ion beam fraction. At higher impact energy two other reaction channels with smaller energy defects also become apparent.

The dominant reaction channel can be explained within a one-electron model, where the 'active' electron is captured because of screened-nucleus–electron interaction,

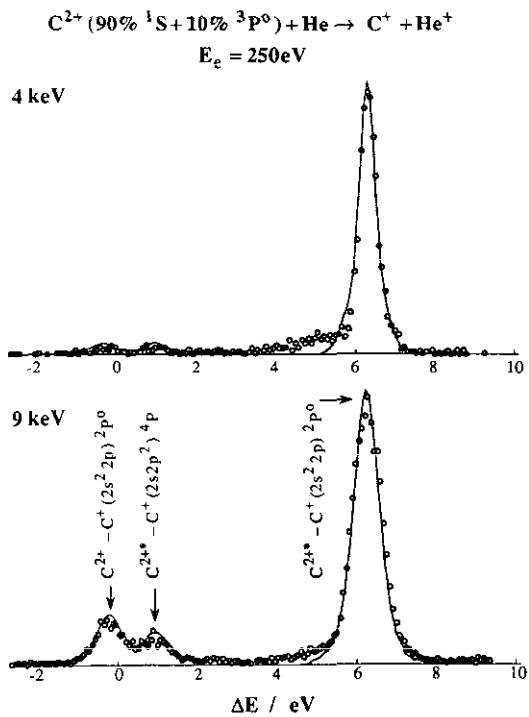

Figure 5. TES for SEC in C^{2+} + He collisions at impact energies of 4 and 9 keV, respectively. The shaded peaks originate from metastable C^{2+} $^3P^o$ primary ions.

whereas all other electrons act as 'spectators'. SEC processes with multicharged ions are commonly discussed with respect to a *reaction window* (Taulbjerg 1986, Schweinzer and Winter 1990a). This reaction window is derived from the Landau–Zener model with analytical fits for the relevant coupling matrix elements (Kimura *et al* 1984), which must be reduced by a 'Taulbjerg-factor' (Taulbjerg 1986) if the projectile ions are only partially stripped.

This concept, if applied to C^{2+}–He collisions in our impact energy range, predicts the maximum for the reaction window between 6.3 and 7.2 eV, which quite satisfactorily explains the dominance of the reaction channel at $\Delta E = 6.3$ eV.

3.3. State-selective measurements for C^{2+}–Ar

Total cross sections for C^{2+}–Ar agree, within the given error limits, with equivalent data for C^{2+}–H_2 (see table 1). Figure 6 shows translational energy spectra (TES) for C^{2+}–Ar at ion impact energies of 2, 4 and 9 keV, with a C^{2+} $^3P^o$ metastable fraction of 10%. All reaction channels have been identified with reference to spectroscopic data

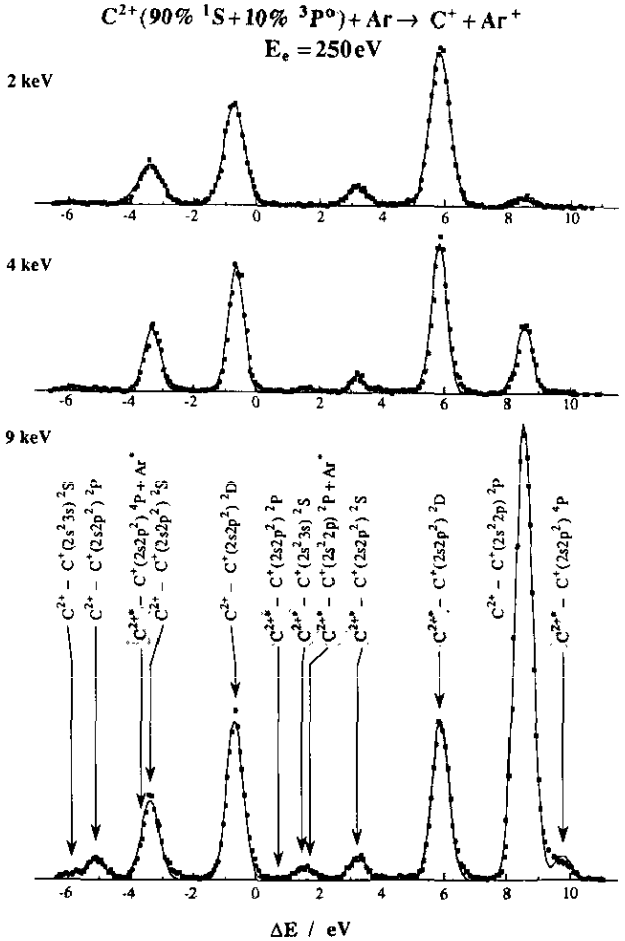

Figure 6. TES for SEC in C^{2+} + Ar collisions at impact energies of 2, 4 and 9 keV. The shaded peaks originate from metastable C^{2+} $^3P^o$ primary ions.

of Bashkin and Stoner (1975, 1978). TES for different impact energies have been normalized to the $C^+(2s2p^2)\ ^2D$ reaction channel ($\Delta E = 5.82$ eV), which represents the dominant contribution to the total SEC cross section for the metastable C^{2+} species. This collision system has already been investigated by Lennon *et al* (1983) who have presented qualitatively similar TES.

Peaks corresponding to reaction channels for metastable primary ions have been shaded in figure 6. Note that for a comparison of involved SEC cross sections these peaks in the TES should be enlarged by about a factor of nine with respect to TES peaks originating from ground-state primary ions.

SEC into $C^{2+}\ ^1S$ ground-state ions obviously populates only C II doublet states, in accordance with the Wigner spin conservation rule (Wigner 1927, Moore 1973, 1974), and $C^+(2s2p^2)\ ^4P$ is only populated by SEC into $C^{2+}\ ^3P^o$, as can be seen from figure 6 (9 keV impact energy). Although production of $C^+(2s2p^2)\ ^4P$ from C^{2+} ground-state ions would involve the much more favourable energy defect of 3.3 eV, such a reaction channel has not been observed, as could be proved by measuring TES with pure ground-state primary ion beams.

All reaction channels seem to correspond to SEC of one 3p electron from Ar, leaving the target ion in its ground state $Ar^+(3s^23p^5)\ ^2P$. Although SEC of a 3s electron from Ar cannot completely be ruled out from our measurements (cf figure 6), it seems to be rather unlikely, since all possibly related reaction channels can also easily be explained by SEC of a 3p electron.

All observed SEC reaction channels (cf figure 6) correspond to processes where the configuration of the open-shell electrons (core-electrons) on the primary ions is either left *unchanged*

$$C^{2+}[(2s^2)\ ^1S;\ (2s2p)\ ^3P^o] + Ar \rightarrow C^+[(2s^2nl)\ ^2L;\ (2s2p^2)\ ^2L] + Ar^+(3s^23p^5)\ ^2P^o \qquad (3)$$

or *changes* during the SEC according to

$$C^{2+}[(2s^2)\ ^1S;\ (2s2p)\ ^3P^o] + Ar \rightarrow C^+[(2s2p^2)\ ^2L;\ (2s^23s)\ ^2S] + Ar^+(3s^23p^5)\ ^2P^o. \qquad (4)$$

SEC processes as described by equation 3 are genuine *one-electron processes* (cf Schweinzer and Winter 1990a, b) and might be expected to make up for the dominant SEC contributions.

Practically all reaction channels starting with $C^{2+}\ ^3P^o$ metastable primary ions belong to this class of SEC processes. If applied in our impact energy range to C^{2+}-Ar, the above described modified Landau–Zener concept predicts reaction channels with energy defects from 4.5 to 6.5 eV as dominant. Therefore, SEC into $C^{2+}\ ^3P^o$ should feature larger cross sections than SEC into $C^{2+}\ ^1S$ (cf figure 3 for H_2 target), because the latter primary ions cannot give rise to SEC with energy defects inside the above given reaction window.

SEC into the ground state $C^{2+}\ ^1S$ at low impact energy is dominated by *two-electron* processes according to equation (4) involving endothermic energy defects (cf figure 6). Theoretical treatment of such endothermic SEC reactions requires a more detailed knowledge of potential energy curves of the collisional quasimolecule for internuclear distances $R < 4a_0$. However, a qualitative explanation for these two-electron transitions will be presented in the following.

Generally, a two-electron process might either be caused by two subsequent, mutually independent one-electron transitions due to nucleus–electron interaction or screening effects or, on the other hand, by a single correlated two-electron transition. The latter mechanism is not covered by the commonly used independent particle model

(IPM) for ion–atom collisions, which postulates that each electron moves independently of all the others in a potential representing the attraction of the nuclei and the average repulsive effect of all other electrons. A review of electron correlation in ion–atom collisions has recently been given by Stolterfoht (1990), to which the reader is referred for further details.

For SEC in collisions of C^{2+} ^1S with Ar, electron capture with excitation of a projectile core electron ($2s \rightarrow 2p$) can either be caused by two successive nuclei–electron interactions (as proposed by the IPM) or in the following way (see also Schweinzer and Winter 1990b).

While the target electron is captured because of nucleus–electron interaction, the excitation process results from electron–electron interaction of the already captured electron with one 2s projectile core electron. In general it is difficult to decide which of the two mechanisms is the more important one. In our case, however, strong evidence for a dominant contribution of electron–electron interaction is suggested from examination of the resulting C II $(2s2p^2)$ ^2S, ^2D final states.

In atomic systems electron correlation is in general related to *configuration mixing* (Condon and Shortley 1970). It is well known (Weiss 1967) that energy levels for the C II $2s2p^2$ configuration cannot be described by a single configuration state. Furthermore, in the C II spectrum two-electron transitions ($(2s2p^2)$ ^2D, ^2S–$(2s^23p)$ $^2P^o$) would be forbidden within the IPM, but are well observed (Nussbaumer and Storey 1981), which can only be due to a breakdown of precise configuration assignment (Condon and Shortley 1970). Dankwort and Trefftz (1977) performed multiconfiguration Hartree–Fock calculations to obtain the mixing parameters for the C II $(2s2p^2)$ ^2S state. The $2s2p^2$ component accounts only for a fraction of 70% in their multiconfiguration state, with $2s^23s$ being the strongest perturbing configuration. SEC to such highly correlated states of C II may take place within an AO-close-coupling description (Schweinzer and Winter 1990a, b) in the following way.

The target electron is captured by nucleus–electron interaction to a single configuration state $2s^2nl$ with $n > 2$ (note that the primary ion core configuration is not yet altered), which however is no eigenstate of the atomic Hamiltonian. This non-stationary state is strongly coupled because of correlation interaction with other single configuration states (e.g. $2s2p^2$), which differ by precisely two spin orbitals. Consequently, this system of coupled states evolves in time and develops asymptotically into stationary multiconfiguration states of C II. In this way electron correlation in the final states increases the probability for two-electron processes.

3.4. State-selective measurements for C^{2+}–H_2

Because of the similar ionization potentials of H_2 (15.42 eV) and Ar (15.76 eV), specified final states of C II can be populated in C^{2+}–Ar and –H_2 collisions with similar energy defects. However, the density of these final states is greatly enhanced in the case of H_2, because after electron capture the resulting H_2^+ ion can be left in various vibrationally excited states ν'. TES for SEC by C^{2+} from respectively Ar (shaded peaks) and H_2 at 4 keV impact energy have been plotted together in figure 7, with the dominant reaction channel for both collision systems normalized to the same height. The energy resolution was not sufficient to permit resolution of the vibrational state population of the resulting molecular target ion. However, a shift of all reaction channels to more endothermic energy defects, corresponding to population of $H_2^+(\nu' > 0)$ states, can clearly be observed. Knowing from C^{2+}–Ar collisions the kinetic energy widths of TES

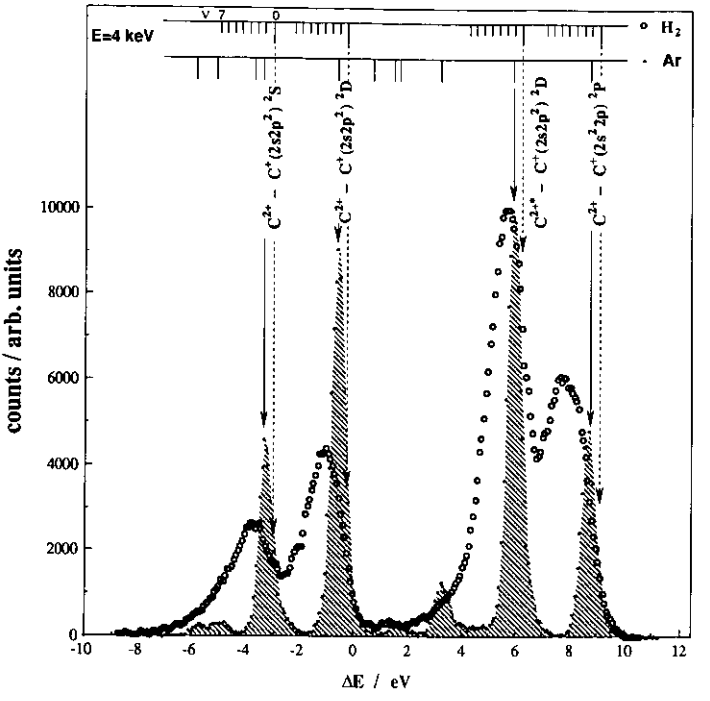

Figure 7. Comparison of TES for SEC in C^{2+} + Ar collisions (shaded) and C^{2+} + H_2 collisions (open symbols) at 4 keV impact energy. The peaks for the H_2 target are broader and shifted towards lower energy defects because the H_2^+ molecular ion becomes vibrationally excited ($\nu' > 0$).

peaks for well defined energy defects, the centre of each ν' distribution could be derived from the TES by means of a fitting procedure (Schweinzer *et al* 1988).

In order to investigate the importance of $H_2 \rightarrow [H_2^+]$ Franck-Condon factors for the SEC process, close-coupling model calculations have been performed with and without taking into account the Franck-Condon principle for ionizing transitions in the molecular target. The model involved one entrance channel (C^{2+} ^1S, $[^3P^o] + H_2$) and 12 product channels (C^+ ^2P, $[^2D] + H_2^+(\nu')$) for the vibrationally excited states with $\nu' = 0$–11. The calculations have only been performed for the exothermic reaction channels shown in figure 7, because treatment of the endothermic channels would involve more detailed knowledge of the corresponding potential energy curves (cf section 3.3).

Regarding the diabatic potential curves, we assumed only Coulomb repulsion for the final states and neglected polarization interaction in the entrance channel. Only coupling of the initial state with all final states has been included in the calculations, whereas recoupling among the final states was neglected. Approximate coupling matrix elements have been derived from a standard formula originally given by Olson and Salop (1976) and modified by Kimura *et al* (1984) and Taulbjerg (1986). Although this formula corresponds to coupling at well defined potential energy curve crossings R_c, we extended its validity to regions around the crossing radii (cf Laurent *et al* 1987).

At keV impact energies the Franck-Condon principle should be obeyed during the SEC process for transitions in the molecular target from $H_2(\nu = 0)$ to $H_2^+(\nu')$, because of the rather short collision time in comparison with a typical vibrational period. Such

transitions are usually called vertical transitions, with their relative intensities being determined by Franck–Condon factors (Halmann and Laulicht 1965), which are defined as the squares of overlap integrals of vibrational wavefunctions for the two involved vibrational levels. For this reason, the corresponding coupling matrix elements H_{12} have to be multiplied with the square roots of the respective Franck–Condon factors f (Olson and Salop 1976).

$$H_{12}^{*} = \sqrt{f} H_{12}. \tag{5}$$

Relevant approximate Franck–Condon factors have been taken from Dunn (1966).

Figure 8 compares our experimental results for the centre of vibrational distributions with results of close-coupling calculations with (AO+FC) and without (AO) inclusion of the Franck–Condon factors. Evidently, our experimental data cannot satisfactorily be explained by exclusive AO calculations, where the calculated distribution is only determined by the energy defect of a certain vibrational level with respect to the reaction window. This would correspond to the population of vibrationally highly excited states of H_2^+ and is in contradiction to our measurements. On the other hand, if Franck–Condon factors are included, good agreement with the experimental data can be achieved, showing that the consideration of these Franck–Condon factors is necessary to explain the observed TES. However, the Franck–Condon principle, which states that the vibrational distributions are determined only by the Franck–Condon factors, is not rigorously fulfilled, because different exothermic reaction channels involve different vibrational distributions, as can be seen from figure 8. Higher vibrational levels are populated for $C^+ {}^2P$ than for $C^+ {}^2D$ final states, apparently due to the influence of the reaction window. Consequently, the resulting vibrational distributions depend on the Franck–Condon factors as well as the energy defects of the particular

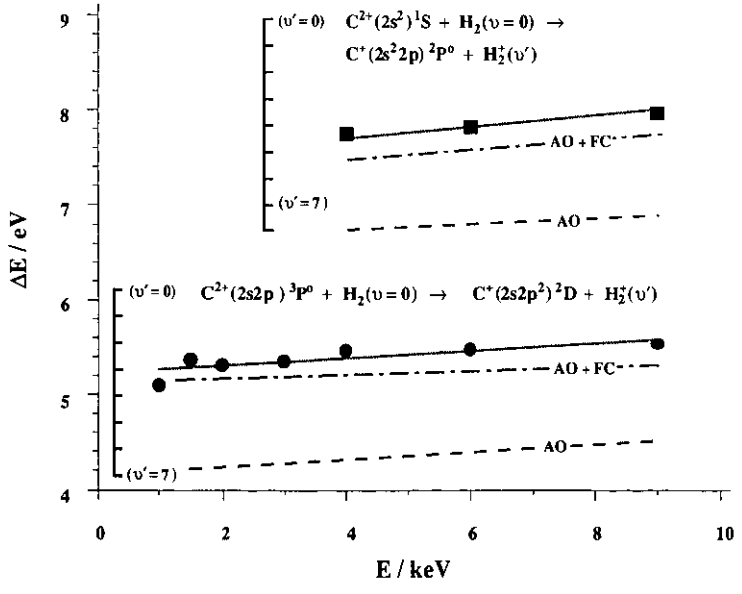

Figure 8. Mean energy defects for the dominant exothermic reaction channels for SEC in $C^{2+} + H_2$ collisions plotted against impact energy. The full symbols belong to the measured TES peak positions, and broken and chain lines denote results of AO calculations without and with consideration of Franck–Condon factors, respectively (cf text for further explanations).

reaction channels with respect to the reaction window. This observation is in agreement with similar studies of other groups (Huber and Kahlert 1985, Fukuroda *et al* 1989).

4. Summary

We have studied single electron capture (SEC) in collisions of 0.5–9 keV C^{2+} with He, H_2 and Ar, based on state-selective information from translational energy spectroscopy and measurement of absolute total SEC cross sections for the C^{2+} ground state as well as the metastable $(2s2p)\ ^3P^o$ state.

In all three collision systems the metastable state gives rise to much larger SEC cross sections than the C^{2+} ground state, from which fact we conclude that earlier studies on SEC in these collision systems without defined metastable primary ion beam fractions are of rather limited significance.

The state-selective measurements showed that for the present collision systems SEC by the C^{2+} metastable ions does not generally change the original primary ion configuration, whereas SEC by the ground-state ions can also be accompanied by a change of the original C^{2+} configuration (core-changing SEC). In general, this behaviour can satisfactorily be explained with the 'reaction window' concept for SEC. The core-changing reactions have been interpreted as correlated two-electron transitions in SEC populated final C^+ states which involve strong configuration mixing.

For SEC from H_2 our findings require the additional consideration of Franck–Condon factors for the H_2^- (H_2^+) transitions, i.e. the SEC induces vibrational excitation of the final target ions in such a way that reaction channels which without this vibrational excitation would involve higher exothermicity than favoured by the corresponding reaction window become shifted nearer to its centre.

Acknowledgments

This work has been supported by Austrian Fonds zur Förderung der wissenschaftlichen Forschung (Project No 5317), and by Kommission zur Koordination der Kernfusionsforschung at the Austrian Academy of Sciences. It was performed within a coordinated research program of the International Atomic Energy Agency on 'Atomic and Molecular Data for Fusion Edge Plasmas'.

References

Armenante M, Santoro V, Spinelli N and Vanoli F 1985 *Int. J. Mass Spectrom. Ion Proc.* **64** 265
Aumayr F, Lakits G and Winter H 1986 *Phys. Rev.* A **33** 846
Aumayr F, Schweinzer J and Winter H 1989 *J. Phys. B: At. Mol. Opt. Phys.* **22** 1027
Aumayr F and Winter H 1985 *Phys. Rev.* A **31** 67
—— 1989 *Phys. Scr.* T **28** 96
Bashkin S and Stoner J O 1975 *Atomic Energy Levels and Grotrian Diagrams* vol 1 (Amsterdam: North-Holland)
—— 1978 *Atomic Energy Levels and Grotrian Diagrams* vol 2 (Amsterdam: North-Holland)
Cheng K T, Kim Y K and Desclaux J P 1979 *At. Data Nucl. Data Tables* **24** 111
Condon E U and Shortley G H 1970 *The Theory of Atomic Spectra* (Cambridge: Cambridge University Press)
Dankwort W and Trefftz E 1977 *J. Phys. B: At. Mol. Phys.* **10** 2541
Dunn G H 1966 *J. Chem. Phys.* **44** 2592

Fukuroda A, Kobayashi N and Kaneko Y 1989 *J. Phys. B: At. Mol. Opt. Phys.* **22** 3457
Gardner L D, Bayfield J E, Koch P M, Sellin I A, Pegg D J, Peterson R S, Mallory M L and Crandall D H 1979 *Phys. Rev.* A **20** 766
Gilbody H B 1978 (Inst. Phys. Conf. Ser. **38**) p 156, ch 4
Gilbody H B, Salin A, Aumayr F, Barany A, Belkic D S, de Heer F J, Hoekstra R, Janev R K, Nakai Y, Rivarola R D, Tawara H and Watanabe T 1989 *Phys. Scr.* T **28** 8
Halmann M and Laulicht I 1965 *J. Chem. Phys.* **43** 1503
Hasted J B and Smith R A 1956 *Proc. R. Soc.* A **235** 354
Herzberg G 1950 *Spectra of Diatomic Molecules* (New York: Van Nostrand Reinhold)
Huber B A and Kahlert H J 1985 *J. Phys. B: At. Mol. Phys.* **18** 491
Janev R K, Harrison M F A and Drawin H W 1989 *Nucl. Fusion* **29** 109
Janev R K, Phaneuf R A and Hunter H T 1988 *At. Data Nucl. Data Tables* **40** 249
Jellen-Wutte Y, Schweinzer J, Vanek W and Winter H 1985 *J. Phys. B: At. Mol. Phys.* **18** L779
Kimura M, Iwai T, Kaneko Y, Kobayashi N, Matsumoto A, Ohtani S, Okuno K, Takagi S, Tawara H and Tsurubuchi S 1984 *J. Phys. Soc. Japan* **53** 2224
Laurent H, Barat M, Gaboriaud M N, Guillemot L and Roncin P 1987 *J. Phys. B: At. Mol. Phys.* **20** 6581
Lennon M, McCullough R W and Gilbody H B 1983 *J. Phys. B: At. Mol. Phys.* **16** 2191
Moore J H 1973 Phys. Rev. A **8** 2359
—— 1974 *Phys. Rev.* A **10** 724
Nakamura T, Kobayashi N and Kaneko Y 1985 *J. Phys. Soc. Japan* **54** 2774
Nussbaumer H and Storey P J 1981 *Astron. Astrophys.* **96** 91
Nutt W L, McCullough R W and Gilbody H B 1978 *J. Phys. B: At. Mol. Phys.* **11** L181
Olson R E and Salop A 1976 *Phys. Rev.* A **14** 576
Phaneuf R A, Meyer F W and McKnight R H 1978 *Phys. Rev.* A **17** 534
Schweinzer J, Jellen-Wutte U, Vanek W, Winter H and Hansen J E 1988 *J. Phys. B: At. Mol. Opt. Phys.* **21** 315
Schweinzer J and Winter H 1989 *J. Phys. B: At. Mol. Opt. Phys.* **22** 893
—— 1990a *J. Phys. B: At. Mol. Opt. Phys.* **23** 3881
—— 1990b *J. Phys. B: At. Mol. Opt. Phys.* **23** 3899
Sherwin C W 1940 *Phys. Rev.* **57** 814
Stangeby P C and McCracken G M 1990 *Nucl. Fusion* **30** 1225
Stier P M and Barnett C F 1956 *Phys. Rev.* **103** 896
Stolterfoht N 1990 *Phys. Scr.* **42** 192
Taulbjerg K 1986 *J. Phys. B: At. Mol. Phys.* **19** L367
Tawara H and Fritsch W 1989 *Phys. Scr.* T **28** 58
Tawara H and Phaneuf R A 1988 *Comment. At. Mol. Phys.* **21** 177
Turner B R, Rutherford J A and Compton D M J 1968 *J. Chem. Phys.* **48** 1602
Weiss A W 1967 *Phys. Rev.* **162** 71
Wigner E 1927 *Nachr. Akad. Wiss. Göttingen, Math.-Phys. Kl.* **IIa** 375